Cytoplasmic delivery of quantum dots *via* microelectrophoresis technique

Mengke Han [1,2], Jiangbo Zhao [1,2], Joseph Mahandas Fabian [3], Samuel Evans [2,4], Sanam Mustafa [2,4], Yinlan Ruan [1,2], Steven Wiederman [2,4] and Heike Ebendorff-Heidepriem [1,2,*]

[1] Institute for Photonics and Advanced Sensing (IPAS) and School of Physical Sciences, The University of Adelaide, Adelaide, South Australia 5005, Australia.

[2] ARC Centre of Excellence for Nanoscale BioPhotonics (CNBP), The University of Adelaide, Adelaide, South Australia 5005, Australia.

[3] Flinders Medical Centre, Flinders University, South Australia 5042, Australia.

[4] Adelaide Medical School, The University of Adelaide, Adelaide, South Australia 5005, Australia.

[*] Correspondence should be addressed to the following author:

Heike Ebendorff-Heidepriem (Professor)

School of Physical Sciences

Institute for Photonics and Advanced Sensing

The University of Adelaide, Adelaide, South Australia 5005, Australia

heike.ebendorff@adelaide.edu.au

Keywords: *Intracellular delivery, Microelectrophoresis, Nanoparticles, Quantum dots, Biosensor*

Abstract: Nanoparticles with specific properties and functions have been developed for various biomedical research applications, such as *in vivo* and *in vitro* sensors, imaging agents and delivery vehicles of therapeutics. The development of an effective delivery method of nanoparticles into the intracellular environment is challenging and success in this endeavor would be beneficial to many biological studies. Here, the well-established microelectrophoresis technique was applied for the first time to deliver nanoparticles into living cells. An optimal protocol was explored to prepare semiconductive quantum dots suspensions having high monodispersity with average hydrodynamic diameter of 13.2 - 35.0 nm. Micropipettes were fabricated to have inner tip diameters of approx. 200 nm that are larger than quantum dots for ejection but less than 500 nm to minimize damage to the cell membrane. We demonstrated the successful delivery of quantum dots *via* small electrical currents (-0.2 nA) through micropipettes into the cytoplasm of living human embryonic kidney cells (roughly 20 - 30 µm in length) using microelectrophoresis technique. This method is promising as a simple and general strategy for delivering a variety of nanoparticles into the cellular environment.

1 Introduction

The intracellular delivery of exogenous materials with high efficiency and specificity, has shown great promise in deciphering and even modulating the complex, spatiotemporal interplay of biomolecules within living cells [1,2]. As a powerful technique widely applied in modern biology, microelectrophoresis uses electrical currents to eject charged substances through fine-tipped glass micropipettes into living cells [3]. Microelectrophoresis performs intracellular delivery in a highly controlled manner. It can limit the problematic diffusion of chemically and pharmacologically active substances from micropipettes, by simply applying a retaining current [3], which can reduce cell distortion and damage. In addition, as most biological membranes *in vivo* maintain resting membrane potential differences ranging from -30 to -180 mV [4], microelectrophoresis can readily locate target cells deep in tissue slice or living animals. Once the micropipette is pierced into the cytosol of target cell, it can measure intracellular electrical activity in real-time [5].

Although microelectrophoresis has been established since *circa* 1900 [6], no studies have been conducted to explore the intracellular microelectrophoretic delivery of nanoparticles, despite the rapid development of utilizing nanomaterials in various intracellular biological research and medical applications [2]. For example, fluorescent semiconductive quantum dots (QDs) with superior optical properties and surface groups permit real-time tracking of intracellular molecules over time scales of milliseconds to hours, offering a capability to monitor intracellular events that cannot be accomplished via organic fluorophores. The main challenge confronting microelectrophoretic delivery of nanoparticles is the possibility of nanoparticle aggregation in the tip of micropipettes during ejection, which can cause tip blockage and failed delivery. The reasons are twofold.

Firstly, traditionally used silver/silver chloride (Ag/AgCl) electrodes in microelectrophoresis only conduct well (transform the flow of electrons from the current source to a flow of ions in solution) in solutions that contain substantial Cl^- ions [7]. Accordingly, target cells can be located and subsequently their intracellular electrical activity recorded with high signal to noise ratio and wide recording bandwidth (only for electrically excitable cells, *i.e.,* neurons, muscle cells and some endocrine cells). Therefore, potassium chloride (KCl) solution with concentration of 0.2 - 2 M is typically used to dissolve charged substances to be ejected [3,5]. The concentration of KCl should be as high as possible for low-noise intracellular recording while considering the solubility of different substances. For nanoparticles, high KCl concentration significantly lowers their repulsive energy barrier, *i.e.,* zeta potential at their hydrodynamic diameters, which leads to the irreversible aggregation of nanoparticles [8]. This can cause blockages in the tip of micropipettes during ejection and thus failed microelectrophoresis.

Secondly, to impale cells with minimal damage, a rule of thumb is that the outer diameter (OD) near the tip of micropipettes should be less than 500 nm [3]. However, the inner diameter (ID) near the tip must be large enough to allow the ejection of nanoparticles having comparable hydrodynamic diameters. Tips that are too small will impede the ejection and subsequently cause the aggregation of nanoparticles in the tips, leading to failed microelectrophoresis.

In this paper, we addressed these technical hurdles by preparing optimal nanoparticle suspensions with a low KCl concentration and high pH to reach a compromise between the colloidal stability of nanoparticles for ejection and high-fidelity intracellular recording. In addition, we fabricated micropipettes having appropriate tip sizes to allow the intracellular delivery of nanoparticles into living cells with suitable ejecting current and duration. These results suggest the future potential of microelectrophoresis as a simple and precise approach in the intracellular delivery of various nanoparticles into the cellular environment.

2 Materials and methods

2.1 QDs suspension preparation and colloidal stability measurement

CdSe/ZnS core/shell structured QDs (emission maxima of 655 nm) with amine-derivatized polyethylene glycol (PEG) surface functional group (Q21521MP; Invitrogen), hereafter referred to as 655-QDs, were used to demonstrate intracellular microelectrophoresis. The KCl concentration and pH was adjusted by gradually adding 2 M KCl, 0.1 M Hydrochloric Acid (HCl) or 0.1 M Sodium Hydroxide (NaOH) into QDs suspension in fresh ultrapure water (concentration of QDs was consistently 10 nM). KCl, HCl and NaOH solutions were centrifuged at 4000 revolutions per minute (rpm) for 1 minute before the addition to remove any large-size impurities that can affect measurement results. Zetasizer nano ZSP (Malvern Instruments) was used for the studies on the colloidal stability of 655-QDs as it can measure both the hydrodynamic size of the nanoparticles *via* dynamic light scattering (DLS) and the zeta potential *via* laser Doppler electrophoresis in aqueous media [9]. For the Zetasizer measurements, the Henry's function was set at the value of 1.50 [10]. The dispersant was set to be water (Temperature: 25.0 °C; Viscosity: 0.8872 cP; Refractive Index: 1.330; Dielectric constant: 78.5) and its viscosity was used as the viscosity of the sample. The refractive index and absorption of 655-QDs were set as 2.550 and 0.010 [11].

2.2 Intracellular recording quality test

To determine if the low KCl concentration that is necessary for maintaining the colloidal stability of nanoparticles can permit high-fidelity intracellular recording, we compared the quality of intracellular recordings acquired from dragonflies using standard 2 M KCl, 0.01 M KCl and optimized 655-QDs suspension. With their large head capsule and ease of dissection, dragonflies are an ideal model system for recording *in vivo*, intracellular activity. Wild-caught dragonflies (*Hemicordulia tau*) were immobilized with a mixture of beeswax and gum rosin (solid form of resin) (1:1) on a plastic articulating stage as shown in **Figure 2A**. To gain the access to the brain surface, a small hole was dissected on the posterior surface of the head capsule. A working Ag/AgCl electrode (782500; A-M Systems) was connected to an intracellular bridge mode amplifier (BA-03X; npi electronic) and a counter Ag/AgCl electrode was inserted into the head capsule surface to form a complete electrical circuit. With a pipette holder (PPH-1P-BNC; ALA Scientific Instruments) and a micromanipulator (MM-33; ALA Scientific Instruments), extremely fine-tipped glass micropipettes (pulled by program 1 in **Table 1**) were pierced into single lobula neurons. Neurons were stimulated by drifting small moving visual features across a high refresh rate (165 Hz) LCD monitor placed directly in front of the dragonfly. Data were digitized at 5 kHz with a 16-bit analog-to-digital converter and analyzed off-line with MATLAB. The visual stimulus elicited voltage changes across the cell membranes and the digitized data indicated successful intracellular neuronal recordings in real time.

2.3 Micropipette fabrication

P-97 Flaming/Brown type pipette puller (Sutter Instrument) was used to fabricate micropipettes from aluminosilicate glass capillaries (30-0108; Harvard Apparatus). The pulling programs are listed in **Table 1**. Micropipettes pulled by program 1 were used for intracellular recording on dragonflies. Micropipettes pulled by program 2 were used for microelectrophoresis of QDs. To measure the tip IDs and ODs with high accuracy, fabricated micropipettes were coated with a 3 nm-thick platinum film and fixed in two different orientations onto scanning electron microscope (SEM) stubs: either vertically for tip IDs or horizontally for tip ODs measurement

under a FEI Quanta 450 FEG environmental SEM. Thus, it was not possible to measure both the ID and the OD for the same micropipette tip.

Table 1 The parameters of pulling program 1 and 2 in P-97 puller.

Program			**1**	**2**
Ramp			518	518
Pressure			510	510
Cycle	1	Heat	513	513
		Pull	0	0
		Velocity	8	8
		Time	1	1
	2	Heat	508	440
		Pull	100	100
		Velocity	65	65
		Time	100	100

2.4 Microelectrophoresis

Human embryonic kidney (HEK293) cells were seeded at 80,000 cells/dish onto a low-wall 35 mm imaging dish (80156; ibidi,) and cultured (37°C in a humidified incubator at 5% CO_2) for two days in 1 mL Dulbecco's modified Eagle's media (DMEM) supplemented with 2 mM L-glutamine and 10% fetal bovine serum. During electrophoresis, the media was changed to 2 mL DMEM supplemented with 25 mM HEPES (21063045; Thermo fisher) to maintain physiological pH in atmosphere at room temperature. As shown in **Figure 4A**, HEK293 cells (60-70% confluency) were visualized with 40X water immersion objective of a Nikon Ti-E inverted microscope equipped with cage incubator (Okolab). A stored aliquot of optimized QDs suspension was vortexed for 1 minute and sonicated from 4°C to 24°C without the use of external heat for 30 minutes to fully disperse QDs. The QDs suspension was carefully backfilled into micropipettes via a flexible plastic needle (Warner instruments). The micropipette was inserted with an Ag/AgCl working electrode from the blunt end and was held by a micromanipulator (Sensapex) to slowly move towards a single cell at a 50˚ angle. Another Ag/AgCl counter electrode was carefully placed into the media. The two electrodes were connected to the headstage of the intracellular bridge mode amplifier (BX-01; npi) to form a complete electrical circuit. A change in potential difference around -20 to -40 mV indicated that the tip of micropipette was successfully pierced through the cell membrane into the cytoplasm of the cell. A small current of -0.2 nA was then applied to eject QDs into the cell for 3 minutes.

3 Results

3.1 Optimization of QDs suspension

The impact of KCl concentration on the colloidal stability of 655-QDs was investigated using particle size distribution (DLS technique) and zeta potential measurements. DLS measures the time-dependent fluctuation of scattered light intensity caused by the constant Brownian motion of particles, and reports their hydrodynamic diameters as the equivalent hydrodynamic diameters ($\boldsymbol{D_H}$) of spheres that have the same average diffusion coefficient [12]. An established criterion for monodispersed nanoparticles is that their hydrodynamic diameters ($\boldsymbol{D_H}$) should be less than twice of their diameters in the dry state ($\boldsymbol{D_T}$) measured by transmission electron microscope (TEM) [13]. **Figure 1A** shows the image of 655-QDs (dark dots) on the surface of a TEM grid. The average shape of 655-QDs was modelled as a prolate ellipsoid with the major axis ($\boldsymbol{a_T}$) of 9.7 ± 1.6 nm and the minor axis ($\boldsymbol{b_T}$) of 6.7 ± 0.8 nm (± 1 standard deviation (SD), n = 82) rather than ideal spheres. Therefore,

as per the criterion for nanoparticle monodispersity in aqueous environment, monodispersed 655-QDs should theoretically have major hydrodynamic axes ($\boldsymbol{a_H}$) in the range of 8.1 nm - 22.6 nm and minor hydrodynamic axes ($\boldsymbol{b_H}$) in the range of 5.9 nm - 15.0 nm. To examine the monodispersity of elliptical 655-QDs based on the spherical hydrodynamic diameters reported by DLS technique, the following equation regarding the diffusion properties of anisotropic particles in Brownian motion [14], was used to translate the ellipsoidal dimensions ($\boldsymbol{a_H}$ and $\boldsymbol{b_H}$) of 655-QDs to an equivalent diameter ($\boldsymbol{D_H}$) of spheres having the same diffusion coefficient:

$$\boldsymbol{D_H} = 2 \times \frac{(\boldsymbol{a_H}^2 - \boldsymbol{b_H}^2)^{1/2}}{\ln\left(\frac{\boldsymbol{a_H} + \left(\boldsymbol{a_H}^2 - \boldsymbol{b_H}^2\right)^{1/2}}{\boldsymbol{b_H}}\right)}$$

In view of the range of $\boldsymbol{a_H}$ and $\boldsymbol{b_H}$ dimensions, monodispersed 655-QDs were considered to have hydrodynamic diameters $\boldsymbol{D_H}$ over 13.2 nm and less than 35.0 nm.

Figure 1B compares the scattered light intensity of particles across a range of sizes in 0.01 M and 2 M KCl solutions. The dotted lines indicate the size range of monodispersed 655-QDs from 13.2 to 35.0 nm. In 2 M KCl, QDs completely aggregated with a mean size around 1.5 µm due to the strong electrostatic screening effect caused by the high electrolyte concentration [8]. Whereas in 0.01 M KCl, only 59.2 % of the scattered light came from QDs aggregates or artefacts (*e.g.,* dust). Scattered light intensity is proportional to the sixth power of the particle radius and therefore the intensity-based size distribution is highly sensitive to very small numbers of aggregates or dust [15]. Thus, the number of QDs aggregates in 0.01M KCl was negligible compared to the total number of particles in the sample (determined using Mie theory, as shown in **Figure 1C**) [15]. Since the intensity-based size distribution is more reliable than number distribution, **Figure 1D** (red line) shows the change in the fraction of light intensity scattered by monodispersed 655-QDs (*i.e.,* portion of single QDs) with increasing KCl concentration. It sharply decreased from 40.8 % in 0.01 M KCl to 7.5 % in 0.1 M KCl. Note that there is no data on ultrapure water since the thickness of the electrical double layer of all particles is considered to be about 1 µm [16], making nanoscale particle size distribution measurement in solution *via* DLS impossible.

The negative effect of KCl on the colloidal stability of 655-QDs revealed by DLS was also evidenced by zeta potential measurements. 655-QDs exhibited negative surface charge in ultrapure water, *i.e.,* 0 M KCl, leading to an average zeta potential of -29.9 mV (as shown in **Figure 1D**, blue line). Whereas with increasing KCl concentration, the zeta potential (colloidal stability of 655-QDs) rapidly approached zero due to the stronger electrostatic screening effect [8]. The zeta potential of -29.9 mV for 0 M KCl agrees with a previous report on the zeta potential of gold nanoparticles that are also surface-functionalized with amine-derivatized PEG [17].

The measurements of the zeta potential and size distribution of 655-QDs in different KCl solutions (**Figure 1D**) show that a KCl concentration as low as 0.01 M is most suitable for achieving high zeta potential (absolute value), which is essential to maintain colloidal stability. However, the zeta potential of -7.4 mV for 655-QDs in 0.01 M KCl solution is still not sufficiently high (absolute value) considering that particles with zeta potential more positive than 30 mV or more negative than -30 mV are generally considered to represent sufficient repulsion to maintain their colloidal stability [9]. Thus, we investigated the effect of pH adjustment on the zeta potential of 655-QDs and evaluated its capability to further stabilize 655-QDs.

We commenced with testing impact of pH for QDs suspended in ultrapure water, *i.e.,* 0 M KCl (**Figure 1E**, black line). The as-prepared QD suspension (without pH adjustment) had a pH of ~7 and a zeta potential of -16.6 mV. Note that this zeta potential value (-16.6 mV) was different to that of the QD suspension in ultrapure water used for the study of the impact of KCl concentration (-29.9 mV). This difference was attributed to the large uncertainty of zeta potential measurements in ultrapure water due to low conductivity. The increase of the pH by addition of alkali (NaOH) resulted in a more negative charge for 655-QDs particles (decreased zeta

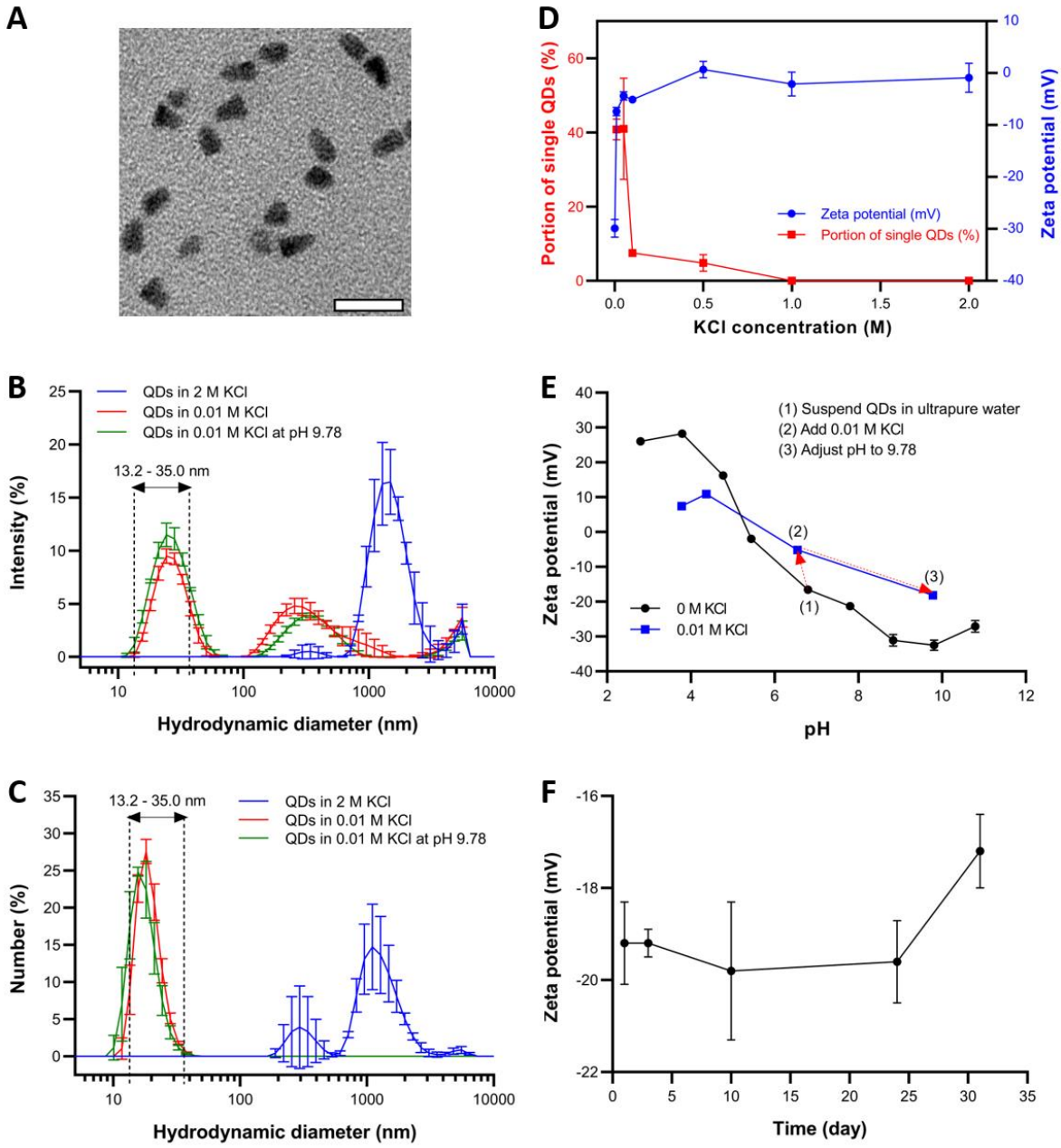

Figure 1 (A) TEM image of 655-QDs reveals an average shape of prolate ellipsoid with a major axis (a_T) of 9.7 ± 1.6 nm and a minor axis (b_T) of 6.7 ± 0.8 nm (± 1 SD with n = 82). Scale bar, 25 nm. **(B)** the size distribution by intensity and **(C)** by number of 655-QDs in 2 M KCl (pH 5.21), 0.01 M (pH 6.55) and optimized suspensions (0.01 M KCl adjusted to pH 9.78). Each data point comprises 12 repeat measurements of 3 independent samples (Error bars, ± 1 SD with n = 3). The dot lines indicate the size range of monodispersed 655-QDs from 13.2 to 35.0 nm. **(D)** the zeta potential of 655-QDs and the portion of singe QDs (determined as fraction of light intensity scattered by monodispersed 655-QDs) as a function of KCl concentration. Error bars, ± 1 SD with n = 3. **(E)** the zeta potential of 655-QDs in ultrapure water and 0.01 M KCl solution with different pH values. Error bars, ± 1 SD with n = 3. Inserted with each step of the optimal preparation process of 655-QDs suspension for microelectrophoresis. **(F)** the stability of 655-QDs zeta potential in optimized suspension. Error bars, ± 1 SD with n = 3.

potential). Conversely, the decrease of the pH by addition of acid (HCl) increased the zeta potential. The most stable state of 655-QDs was achieved by adjusting the pH of QDs suspension to 9.81, where the maximal zeta potential (absolute value) of -32.5 mV was obtained.

Next, we investigated the impact of pH for QDs suspended in 0.01 M KCl solution (**Figure 1E**, blue line). Without pH adjustment, the QD suspension had a zeta potential of -5.2 mV and a pH of 6.55. For lower pH of 3.78 and 4.37, the zeta potential increased to +7.4 and +10.9 mV, respectively. For higher pH of 9.78, the zeta potential decreased to -18.2 mV. These results show that both lower and higher pH can enhance the absolute value of the zeta potential and thus the colloidal stability compared to the QD suspension without pH adjustment. Thus, pH adjustment can effectively buffer the negative effect of 0.01 M KCl on the stability of 655-QDs.

Although a stable state of 655-QDs also exists at acid pH, a strong acid environment (pH<4) is not recommended by the supplier, as the polymer coating can dissociate, exposing and dissolving the core/shell structure. In addition, due to the high mobility of hydrogen ions (H^+), a large amount of H^+ in microelectrophoresis can result in lowering of the pH in the vicinity of the tip of micropipettes [18]. This localized change in pH has been proposed to excite the cell undergoing intracellular recording and interfere with the normal physiological state [19]. On the contrary, 655-QDs do not degrade in a strong basic environment (pH>9) as noted by the supplier. Furthermore, in comparison to the electrophoretic mobility of H^+ (36.25 μmcm/Vs in water at 25.0 °C), hydroxide ion (OH^-) has a lower electrophoretic mobility (20.50 μm cm/Vs in water at 25.0 °C), resulting in less effect on the intracellular activity [20].

Based on the investigation of KCl concentration and pH adjustment on the colloidal stability of QDs, we established the following optimal protocol for the preparation of QDs suspension for microelectrophoresis. The method is to initially dilute QDs stock solution with fresh ultrapure water to 10 nM and then gradually add 2 M KCl to the suspension until a final KCl concentration of 0.01 M achieved. Finally, the pH is adjusted to 9.78 by gradually adding freshly prepared 0.1 M NaOH to further stabilize QDs (indicated by dashed red lines with arrow in **Figure 1E**). The green curve in **Figure 1B** shows the size distribution of optimized 655-QDs suspension, where 53.9 % of scattered light comes from monodispersed QDs that constitute 91.4 % of the total number of particles in the sample as **Figure 1C** shows.

For practical microelectrophoresis applications, preparation of fresh suspensions would be too time-consuming. A stock suspension with good colloidal stability and ready for use would be highly beneficial. **Figure 1F** shows the shelf life of optimized 655-QDs suspensions (0.01 M KCl at pH 9.78). They were aliquoted and stored at 4.0 °C in dark. The zeta potential values of QDs in these intact aliquots were measured on different days, which remained the same for at least 24 days, indicative of this beneficial, long-term colloidal stability.

3.2 The effect of KCl concentration on the quality of intracellular recording

The highest KCl concentration suitable to maintain colloidal stability of QDs was determined to be 0.01 M, which raised the problem whether such a low electrolyte concentration and the existence of 655-QDs in optimized suspensions allow for the recording of intracellular activity with sufficiently high fidelity in real-time. Thus, we compared the quality of intracellular recordings acquired by 2 M KCl solution (used in standard dragonfly electrophysiology) with those of 0.01 M KCl solution and optimized 655-QDs suspension (0.01 M KCl at pH 9.78). The intracellular recordings were captured from visual neurons, binocular small target motion detector (BSTMD2), in the optic lobes of living dragonflies [21]. When BSTMD2 is presented with a small drifting target, the cell responds by significantly increasing the frequency of action potential firing.

Figure 2B shows the typical raw responses (left panel) and an enlarged view of individual spike waveforms (right panel) recorded by 2 M KCl, 0.01 M KCl and optimized 655-QDs suspension from BSTMD2 cells (n = 6) presented with a small moving target. The average tip resistance for micropipettes filled with 2 M KCl, 0.01 M KCl and optimized 655-QDs suspension was 120 MΩ, 335 MΩ and 300 MΩ, respectively. Although the recordings acquired by using low KCl concentration (0.01 M KCl without QDs and optimized 655-QDs suspension) had a greater degree of variation in quality (*i.e.,* noise and signal amplitude) than the recordings acquired by 2 M KCl, it was possible to count spikes that were distinct from the resting potential without any

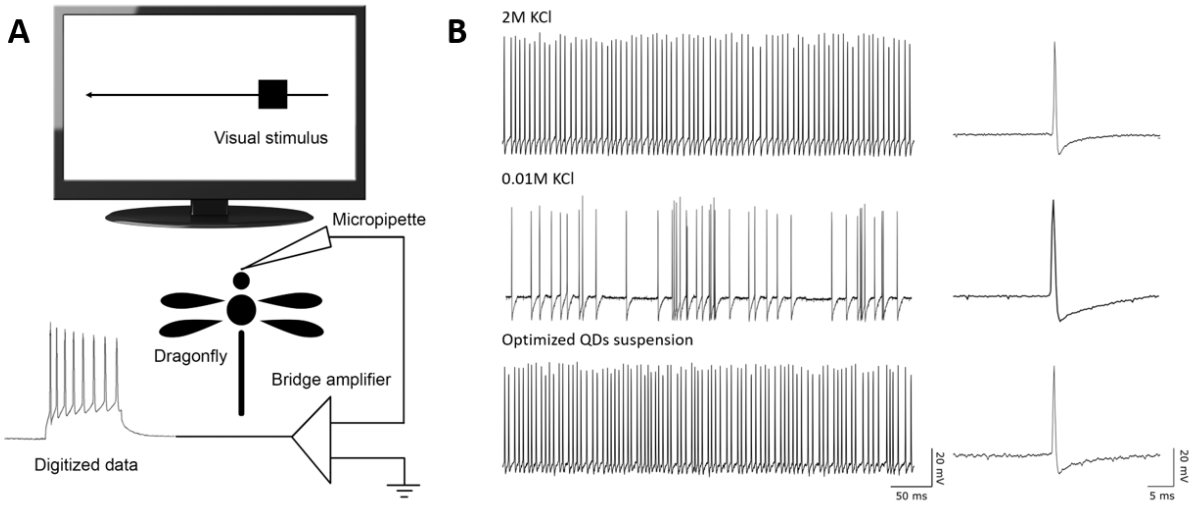

Figure 2 (A) schematic illustration of the experiment setup for intracellular recording of dragonflies. A liquid crystal display (LCD) monitor was placed in front of the dragonfly for stimulating visual neurons by drifting small moving objects. The visual stimulus elicited voltage changes across the cell membranes of single lobula neurons, which were recorded in real-time. **(B)** the responses of two BSTMD2 cells in two separate dragonflies to the presentation of a drifting object, which were recorded with micropipettes filled with 2 M KCl solution, 0.01M KCl solution and optimized 655-QDs suspension (0.01 M KCl at pH 9.78).

issue in temporal responsiveness. In addition, spiking responses and individual action potential waveforms remained very similar for all cases.

As a conclusion, KCl concentration of 0.01 M and the existence of 655-QDs in suspensions can precisely locate target cells, and then produce high-fidelity intracellular recordings.

3.3 Optimizing the tip size of micropipette for intracellular delivery

For successful microelectrophoresis, the tip ID of the micropipette is required to be larger than the sum of hydrodynamic diameters of nanoparticles and other dissolved ions that pass through the tip for conductivity. The range of hydrodynamic diameter of monodispersed 655-QDs is 13.2 - 35.0 nm. The theoretical hydrated diameters of K^+, Cl^- and Na^+ ions are 0.3, 0.4 and 0.2 nm, respectively [22]. Considering the unavoidable trace amount of QDs aggregates or artefacts (*e.g.,* dust) existing in the optimized QDs suspension (**Figure 1B**), the tip ID of the micropipette should be as large as possible to eliminate tip blockage. However, as proposed by previous studies, the tip OD should be less than 500 nm to avoid physical damage to living cells [3]. To achieve small tip OD yet large enough tip ID, we chose aluminosilicate glass for the fabrication of micropipettes since a unique characteristic of aluminosilicate micropipettes is that the ratio of their ID to OD increases remarkably towards the tip [23]. Thus, they have extremely thin wall near the tip, which provides the smallest possible tip OD to avoid physical damage to cells.

The pulling program 1 listed in **Table 1** was designed to fabricate micropipettes with tip ID of *ca.* 100 nm in previous studies of standard dragonfly electrophysiology [24]. To achieve larger tip ID suitable for QDs ejection, we reduced the heat value in the second cycle from 508 in program 1 to 440 in program 2. **Figure 3** shows the SEM images of aluminosilicate micropipettes pulled by program 2 in front and side views. The average tip OD of 26 fabricated micropipettes was 202 nm with a tolerance of ± 35 nm (± 1 SD). The average tip ID of another 26 micropipettes was 206 nm with a larger tolerance of ± 46 nm (± 1 SD). These two averages were nearly identical, which validated the unique characteristics of aluminosilicate micropipettes. Their extremely thin wall near the tip made the tip OD as small as possible to minimize the physical damage to cell membrane while having large enough tip ID for the ejection. The average tip ID of approx. 200 nm was the maximum achievable size by lowering the heat value in the second cycle. For lower heat values, the aluminosilicate capillaries did not soften sufficiently to form micropipettes. The variance was in part caused by the

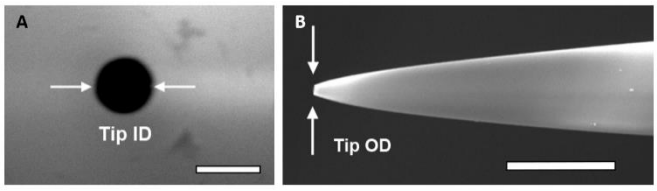

Figure 3 (A) high resolution SEM image of a micropipette for microelectrophoresis of 655-QDs with a tip ID of 211 nm (front view). The orifice of micropipette is the black circle near the centre of the image. Scale bar, 250 nm. **(B)** high resolution SEM image of another micropipette (pulled with program 2) with a tip OD of 212 nm (side view). Scale bar, 2.5 µm.

observational error due to the inconsistency of pipette angle when manually fixing micropipettes onto the vertical SEM sample holder. In addition, when pulling micropipettes, capillaries with slightly different IDs (0.52 ± 0.03 mm, ± 1 SD, n=26) and ODs (0.99 ± 0.02 mm, ± 1 SD, n=26), had different distances to the box heating filament and different volume of air enclosed in the internal channel, which altered the glass temperature and resulted in variations in tip ID and OD of micropipettes [25].

In summary, the range of tip IDs of our aluminosilicate micropipettes is suitable for the ejection of 655-QDs and the tip ODs are less than 500 nm to avoid physical damage to cells as proposed by previous studies [3].

3.4 Successful cytoplasmic delivery of QDs into living cells *via* microelectrophoresis

Figure 4B shows the differential interference contrast (DIC), fluorescent and overlay images of the typical results after microelectrophoresis delivery of 655-QDs into HEK cells (n=20). QDs evenly dispersed throughout the cytoplasm without entering the nucleus. During microelectrophoresis, the resistance of micropipettes was frequently measured to confirm that there was no blockage or breakage in the tips. The resistance of several micropipettes varied from 50 MΩ to 80 MΩ due to the variation in their tip sizes and remained the same when removed out of the cells after delivery, which indicated that there was no tip blockage or breakage happened during microelectrophoresis.

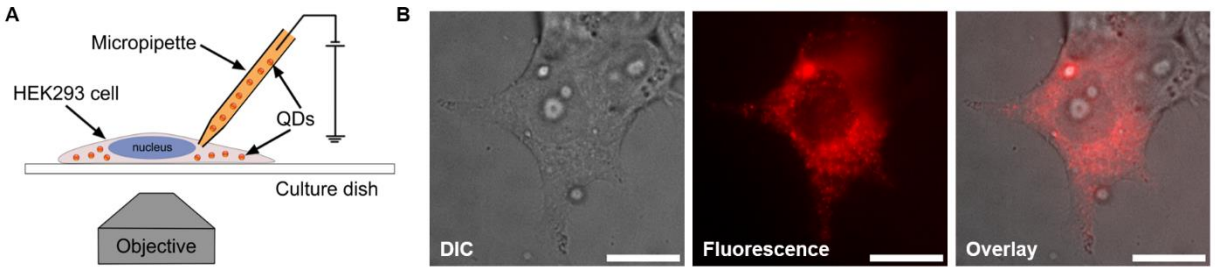

Figure 4 (A) diagram of microelectrophoresis of 655-QDs into HEK293 cells. **(B)** DIC, fluorescence, and overlay images of a HEK293 cell with microelectrophoretic-delivered 655-QDs. The red dots in the cytoplasm are 655-QDs. Scale bar, 10 µm.

4 Concluding remarks

We demonstrated for the first time the use of the well-established microelectrophoresis technique for the successful delivery of nanoparticles, such as QDs used here, into the cytoplasm of living cells. This was achieved by overcoming the following two critical challenges. Firstly, we prepared QDs suspensions with low KCl concentration and high pH value, which maintained high QDs colloidal stability to prevent aggregation and blockages in the tip of micropipettes during ejection, while being able to record the intracellular electrical activity of dragonfly neurons with high fidelity. Secondly, we fabricated micropipettes with inner tip diameters of approx.

200 nm, which was large enough to allow the ejection of QDs and less than 500 nm to avoid physical damage to HEK293 cells as proposed by previous studies [3]. This successful microelectrophoretic ejection of QDs lays the foundation for further studies and applications of microelectrophoresis technique for the intracellular delivery of various nanoparticles.

This work was performed in part at the Optofab node of the Australian National Fabrication Facility (ANFF) utilizing Commonwealth and SA State Government funding. The authors acknowledge partial support from the Australian Research Council Centre of Excellence for Nanoscale BioPhotonics (CNBP) (CE140100003) and Discovery Early Career Researcher Award (DECRA) from Australian Research Council (ARC) (DE150100548). M.H. thanks K. Neubauer, A. Slattery and J. Sibbons for their assistance in SEM, TEM, live cell microscopy at Adelaide Microscopy.

The authors have declared no conflict of interest.

The data that support the findings of this study are available from the corresponding author upon reasonable request.

5 References

[1] Stewart, M. P., Sharei, A., Ding, X., Sahay, G., Langer, R., Jensen, K. F., *Nature* 2016, *538,* 183-192.
[2] Chou, L. Y., Ming, K., Chan, W. C., *Chem. Soc. Rev.* 2011, *40,* 233-245.
[3] Curtis, D. R., *Microelectrophoresis*, New York: Academic Press, 1964.
[4] Tekle, E., Astumian, R. D., Chock, P. B., *Biochem. Biophys. Res. Commun.* 1990, *172,* 282-287.
[5] Mobbs, P., Becker, D., Williamson, R., Bate, M., Warner, A., Techniques for dye injection and cell labelling, in Proceedings of the *Microelectrode techniques. The Plymouth workshop handbook. Cambridge, UK: The Company of Biologists Ltd*, 1994, 361-387.
[6] Lalley, P. M., U. Windhorst, H. Johansson (Eds.),in: *Modern Techniques in Neuroscience Research*, Springer Berlin Heidelberg, Berlin, Heidelberg 1999, p. 193-212.
[7] Axon Instruments, I., *The Axon guide for electrophysiology & biophysics laboratory techniques*, Axon Instruments, 1993.
[8] Zhang, W.,in: *Nanomaterial: Advances in Experimental Medicine and Biology* 2014, p. 19-43.
[9] Clogston, J. D., Patri, A. K., S.E. McNeil (Ed.),in: *Characterization of Nanoparticles Intended for Drug Delivery*, Humana Press, Totowa, NJ 2011, p. 63-70.
[10] Henry, D., The cataphoresis of suspended particles. Part I. The equation of cataphoresis, in Proceedings of the *Proceedings of the Royal Society of London A: Mathematical, Physical and Engineering Sciences*, 1931, 133, 106-129.
[11] Hondow, N., Brydson, R., Wang, P., Holton, M. D., Brown, M. R., Rees, P., Summers, H. D., Brown, A., *J. Nanopart. Res.* 2012, *14,* 1-15.
[12] Pecora, R., *Dynamic light scattering: applications of photon correlation spectroscopy*, Springer Science & Business Media, 2013.
[13] Moon, J., Choi, K.-S., Kim, B., Yoon, K.-H., Seong, T.-Y., Woo, K., *J. Phys. Chem. C* 2009, *113,* 7114-7119.
[14] Perrin, F., *J. Phys. Radium* 1936, *7,* 1-11.
[15] Mie, G., *Ann. Phys. (Berlin, Ger.)* 1908, *330,* 377-445.
[16] Israelachvili, J. N., *Intermolecular and surface forces*, Academic press, 2011.
[17] Xia, X., Yang, M., Wang, Y., Zheng, Y., Li, Q., Chen, J., Xia, Y., *ACS Nano* 2012, *6,* 512-522.
[18] Gruol, D. L., Barker, J. L., Huang, L. Y., MacDonald, J. F., Smith, T. G., Jr., *Brain Res* 1980, *183,* 247-252.
[19] Frederickson, R. C., Jordan, L. M., Phillis, J. W., *Brain Res* 1971, *35,* 556-560.
[20] Duso, A. B., Chen, D. D. Y., *Anal. Chem.* 2002, *74,* 2938-2942.
[21] O'Carroll, D., *Nature* 1993, *362,* 541-543.
[22] Marcus, Y., *Chem. Rev.* 1988, *88,* 1475-1498.
[23] Instrument, S., *P-97 Pipette Cookbook*, 2008.
[24] O'Carroll, D. C., Biomimetic visual detection based on insect neurobiology, in Proceedings of the *Electronics and Structures for MEMS II*, 2001, 4591, 1-11.
[25] Chen, M. J., Stokes, Y. M., Buchak, P., Crowdy, D. G., Foo, H. T., Dowler, A., Ebendorff-Heidepriem, H., *Opt. Mater. Express* 2016, *6,* 166-180.